The Effects of Nature-Inspired Synthesis on Silver Nanoparticle Generation

Zuzana Šimonová,* Veronika Krbečková, Zuzana Vilamová, Edmund Dobročka, Bořivoj Klejdus, Miroslav Cieslar, Ladislav Svoboda, Jiří Bednář, Richard Dvorský, and Jana Seidlerová

ACCESS | Metrics & More | Article Recommendations | Supporting Information

ABSTRACT: A wide range of methods can be used for nature-inspired metallic nanoparticle (NP) synthesis. These syntheses, however, are ongoing in the presence of diverse mixtures of different chemical compounds, and all or only a few of these contribute to resultant particle properties. Herein, the linden (*Tilia* sp.) inflorescence leachate and pure citric and protocatechuic acids were chosen for Ag-AgCl nanoparticle (NP) synthesis, and the resultant particles were then compared. We focused on the following four issues: (1) preparation of Ag-AgCl NPs using the *Tilia* sp.-based phytosynthetic protocol, (2) analytical determination of the common phenolic, nonphenolic, and inorganic profiles of three *Tilia* sp. types from different harvesting locations, (3) preparation of Ag-AgCl NPs using a mixture of citric and protocatechuic acids based on chromatographic evaluation, and (4) comparison of *Tilia*-based and organic acid-based syntheses. Our research confirms that the *Tilia* organic and inorganic profiles in biomasses are influenced by the harvesting location, and the three sites influenced both the morphology and final NP size. Our processing method was uniform, and this enabled great Ag-AgCl NP reproducibility for each specific biomass. We were then able to prove that the simplified organic acid-based synthesis produced even smaller NPs than *Tilia*-based synthesis. These findings provide better understanding of the significant influence on NP final properties resulting from other organic acids contained in the linden.
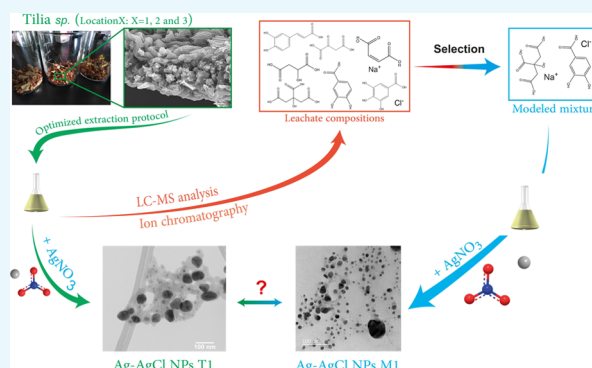
INTRODUCTION

Nature provides a constant source of inspiration and still highly influences scientists in the fields of micro- and nano-technology.[1] Biological structures such as living cells contain nucleic acids, proteins, lipids, polysaccharides, and other storage materials, and these functional macromolecules are built in specific 3D configurations.

The biogenesis of plant nucleic acids, amino acids, proteins, polysaccharides, and some carboxylic acids participates in processes called primary metabolism;[2] however, the biogenesis is also supplemented by nonvital biochemical reactions. These processes differ from species to species, and reactions are referred to as secondary metabolism. The group of the most important secondary metabolites includes alkaloids and phenolic compounds such as flavonoids and terpenoids,[3,4] and their content strongly correlates with plant antioxidant activity,[5] with other influences, including water sufficiency, the amount of available light, frost, wind, and parasite infestation.

The linden (*Tilia* sp.) biomass has a content of the characteristic polyphenols and flavonoids. For example, rutin, quercitrin, kaempferol glycosides, tyliroside, and simple acids such as caffeic, *p*-coumaric, and chlorogenic acids were identified. Some of the authors also confirmed the presence of polysaccharides, condensed tannins, and terpenoids[5–7] and the presence of simple organic acids such as malic, citric, and succinic acids.[8] The molecules contain parts with specific groups, including negatively charged groups (e.g., hydroxyl and carboxyl), and these groups seem to be important for other chemical interactions with external elements.[9,10]

When functional groups and an external metal salt precursor are combined, metal ions are reduced to zero valent or oxide forms.[11,12] Biosynthesis is a technique for different prepara-tions of NPs. Various NP shapes are documented, whether spherical,[13] triangular,[14] or hexagonal,[15] and the color change in the colloidal solution is mostly observed. For example, the Au NP solution is dark red or purple and the Ag NPs colloid is often orange or brown; however, the color is influenced by the NP sizes.[16]

Phytosynthesis is a subcategory of biosynthesis, during which plant leachates or extracts are mainly used. These leachates/extracts are rich in a large number of various organic molecules, and in their structures are such functional groups that interact with external metal ions.[9,10,17] This provides simplicity in biomass input, enables synthesis of many metallic NPs, and effectively controls NP configuration for specific applications. The method, however, has limitations due to its complexity and consequent prediction of the NP synthesis mechanism.

Herein, we focus on (1) chromatographic evaluation of the common phenolic, nonphenolic, and inorganic profiles of the linden (*Tilia* sp.) biomasses harvested in three experimental locations, (2) determining the influence of leachate composition on the final nanometallic colloids, (3) preparation of Ag-AgCl NPs using a mixture of citric and protocatechuic acids based on chromatographic evaluation, and (4) comparison of *Tilia*-based and organic acid-based NP syntheses.

The novelty of this study is apparent in our comparison of Ag-AgCl NPs' characteristics in similar biomass from different harvest locations, the design of the phytosynthesis mechanism based on metabolic and inorganic profiling, and the comparison of the reaction conditions using natural leachate and modeled pure organic mixtures to predict the NPs' final size and morphology.

■ RESULTS AND DISCUSSION

Chromatography Evaluation. *Study of Leachate Compositions.* L1−L3 leachates were examined prior to phytosynthesis using chromatography techniques. The ion chromatography analysis confirmed the presence of sulfates and chlorides (Table 1) and their concentrations differed.

Table 1. Ion Chromatography Results for Inorganic Elements

linden sample	sulfate [mg·L^{-1}]	chloride [mg·L^{-1}]
L1	9 ± 2	16 ± 3
L2	9 ± 2	17 ± 3
L3	6 ± 12	32 ± 7
L-like sample		chloride [mg·L^{-1}]
M1		17 ± 4
M2		17 ± 4
M3		35 ± 8

Sulfate concentrations ranged from 6 to 9 mg·L^{-1}, and concentrations changed even in groups with the same biomass. The L3 biomass had the lowest sulfate content; however, it had the highest Cl$^-$ content. The values for each sample are listed in Table S1 in the Supporting Information.

The presence of Na$^+$, Cl$^-$, N, and P elements was confirmed in linden biomass, and their origin is both natural and anthropogenic. The Cl$^-$ ions are accepted by roots and also by leaves in the form of gases. Moreover, soil properties and excessive salinity influence changes in macro- and micro-nutrient uptake and balance.[18] In this study, the observed high salinity was most likely caused by the increase in the Na$^+$, K$^+$, and Fe^{2+} presence, and the overall plant growth of *Acer platanoides* L. and *Tilia cordata* Mill. was significantly influenced by disturbances in Ca^{2+} and Mg^{2+} ionic ratios.[19] Other influences include lack of water, frost, light conditions, wind, and parasite infestation.[20,21] In addition, sulfate uptake is strongly influenced by the presence of different anions in the

soil solution, and while nitrates stimulate intake, Cl$^-$ anions inhibit it.[22,23]

Both organic phytochemicals and inorganic fractions influence synthetic processes, and we therefore approximated the leachate in two large groups of organic compounds. Herein, basic organic compounds were determined by the liquid chromatography with mass spectroscopy (LC−MS) technique. In total, 32 compounds were identified, of which 17 were "phenolic" and 15 were "nonphenolic" carboxyl acids. Table S2 in the Supporting Information lists the specific components. The highest content of nonphenolic acids was found in leachates prepared from L2 biomass. Then, L1 leachates followed, and the lowest nonphenolic acid content had L3 samples. On the other hand, the highest proportion of phenolic acids contained L1 samples, followed by L2 and L3.

Table 2 shows the selected candidates probably involved in the synthesis of NPs. Significant differences in the measured

Table 2. Organic Compounds in Linden-Based Leachates Are Present in μg·g^{-1} of DW[a]

leachate	citric acid [μg·g^{-1}]	maleic acid [μg·g^{-1}]	malic acid [μg·g^{-1}]	oxaloacetic acid [μg·g^{-1}]
L1	1935 ± 67	2459 ± 156	2175 ± 177	152 ± 2
L2	1886 ± 143	2959 ± 298	2601 ± 397	262 ± 42
L3	2126 ± 325	1798 ± 257	1659 ± 247	162 ± 16

leachate	gallic acid [μg·g^{-1}]	protocatechuic acid [μg·g^{-1}]	ferulic acid [μg·g^{-1}]	caffeic acid [μg·g^{-1}]
L1	135 ± 20	478 ± 35	4.2 ± 0.1	5.4 ± 1.2
L2	60 ± 4	217 ± 11	4.0 ± 0.3	1.0 ± 0.2
L3	33 ± 10	123 ± 40	4.3 ± 0.4	0.6 ± 0.1

[a]Nonphenolic acids are present in higher amounts than phenolic acids.

samples were observed; however, the differences in one biomass are within error. While maleic, malic, and citric acids were present at over 1800 μg·g^{-1} concentration, oxaloacetic acid was only present in concentrations from 152 to 262 μg·g^{-1}.

The gallic, protocatechuic, ferulic, and caffeic phenolic acids were present in tens to hundreds of μg·g^{-1}. We estimated the total content of phenolic and nonphenolic acids (based on data in Table S2 in the Supporting Information), and this is presented in Table 3. It is important to emphasize that the choice of both solvent and extraction method strongly influences final extract composition.[24]

Table 3. Summation of Phenolic and Nonphenolic Compounds in μg·g^{-1} of DW Detected in the Prepared Linden Leachates

biomass	nonphenolic compounds [μg·g^{-1}]	phenolics [μg·g^{-1}]
LB1	9333 ± 467	792 ± 40
LB2	10,726 ± 536	370 ± 19
LB3	8609 ± 430	283 ± 14

Some of the described acids and phenolics are already used in the preparation and stabilization of metallic NPs,[25−31] and these may have an overall effect on NP formation. For example, Umadevi et al. considered citric and malic acids as main agents involved in the Ag NP phytosynthesis using *Solanum lycopersicum* extract. They suggested that citric acid was the reducing agent and malic acid was the capping agent,[27]

and their high contents in the dry matter were reported.[32] Here, Ag NPs were synthesized with maleic acid and this was confirmed as an effective capping agent in the preparation of spherical Ag NPs.[30]

Different fundamental pathways in plant metabolism and catabolism involve organic acid as intermediate or end products, for example, the citrate or succinate, which are important in the Krebs cycle in the cell's central energy cycle. The accumulation of organic acids in plant tissues must retain their specific physiological functions,[8,33] and they are then responsible for the taste, flavor, microbial stability, and consistency in plant-derived beverages.

The shikimate metabolic pathway is the main source of polyphenol synthesis. This metabolic pathway provides many secondary plant metabolites such as coumarins, lignins, condensed tannins, and stilbenes.[34] Flavonoids in plants are often accompanied by gallic and ellagic acids derived from hydroxybenzoic acid and by caffeic, ferulic, and coumaric acids derived from hydroxycinnamic acid. The number of hydroxyl groups in molecules influences their activity and primary antioxidant effect,[35,36] and their content also varies during plant growth and development.[37] They are also easily soluble in water or methanol.[5]

Finally, both organic and inorganic portions differ in the observed biomasses, and they must be carefully considered in biosynthetic and phytosynthetic experiments because they create the basic stabilization coating on the NP surface. We consider that the high amount of citric, malic, and maleic acids has the greatest effect on NP reduction and stabilization. Although the amount of phenolic acids is low compared to organic acids, their synthetic potential has been confirmed, and these can act in synergy and contribute to those acids' effect. However, it is mostly important to emphasize that this study focused on specific phenolics and organic acids, and other organic compounds could also have an impact on phytosynthesis and resultant NPs.

Stability, Size Distribution, and Morphology Study of the Linden-Based Samples. Data for individual samples in triplicates and histograms are given in Table S3 and Figure S1 in the Supporting Information, and the average values are described in Table 4.

Table 4. Physical−Chemical Examinations of All Samples[a]

sample	ζ-potential [mV]	size by DLS [nm]		size by TEM [nm]	
Ag1	−27 ± 1	68 ± 3		13 ± 8	46 ± 7
Ag2	−29 ± 1	120 ± 2		10 ± 4	40 ± 9
Ag3	−29 ± 1	665 ± 13			
AgM1	−53 ± 2	34 ± 1	112 ± 3	13 ± 3	24 ± 2
AgM2	−43 ± 1	15 ± 2		6 ± 2	14 ± 3 64 ± 15
AgM3	−40 ± 1	3 ± 0.1		4 ± 1	17 ± 4 44 ± 7

[a]Sample sizes obtained by both DLS and TEM techniques.

Transmission electron microscopy (TEM) analysis confirmed that Ag1 and Ag2 samples had mostly spherical Ag-AgCl NPs (Figure 1a,b). The determined average NP size in the Ag1 sample was 13 ± 8 nm, and the Ag2 sample had 10 ± 4 nm mean core size. The most sizes were in the 5−15 nm range and large particles over 30 nm were also detected (Table 6). The high values were calculated separately because the final mean sizes could be inaccurate.
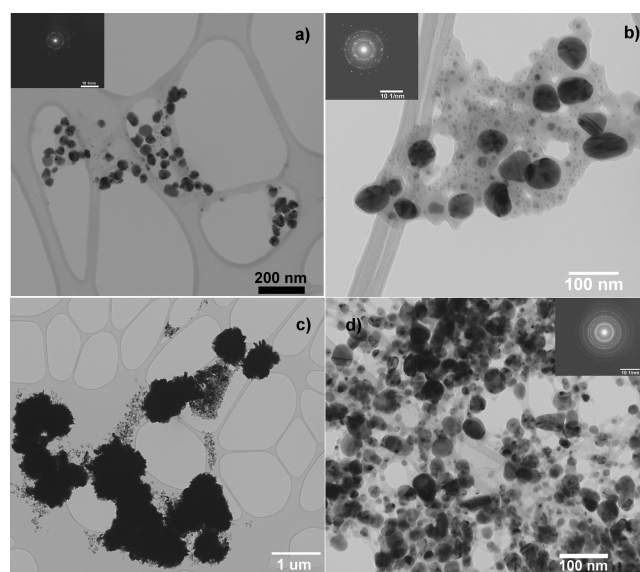

Figure 1. One sample was selected from each triplicate to illustrate the entire sample set. Spherical shapes of Ag1 were confirmed (a), and NPs were crystalline as confirmed by the SAED pattern. Most "core" size diameters were from 5 to 15 nm; however, the fraction of 30−55 nm NPs was also present. The TEM micrographs and histogram of the Ag2 sample are seen on panel (b). The sample has similar nature to Ag1. TEM micrographs of Ag3 (c, d) showed locations with large crystalline objects and sites with a high density of NPs. Size distribution was not calculated because of sample heterogeneity.

Clusters of Ag-AgCl NPs were formed in the presence of organic components of *Tilia* sp.; however, no aggregation was observed. The crystalline nature of the prepared Ag-AgCl NPs was confirmed by selected-area electron diffraction (SAED) patterns, and the crystal twinning typical in silver crystals was also apparent. In our previous study,[38] we used L1 to synthesize Ag NPs for *p*-nitrophenol decomposition. The Ag-AgCl NPs' core diameter was 14 ± 9 nm, and this correlates with these study results. We consider that phytosynthesis using the same biomass and methodology is completely reproducible.

The Ag3 samples presented sites with large crystalline aggregates (Figure 1c) and high NP density (Figure 1d). Because the sample was heterogeneous and the SAED pattern confirmed a predominantly polycrystalline nature, size distribution was not calculated.

The stability of the prepared samples was determined by ζ-potential measurements, and all prepared samples had relatively similar ζ-potential values. The Ag1 sample was determined as the least stable (Table 4), and the ζ-potential of NP was determined to be above −27 mV. ζ-Potential values ranged from −27 to −29 mV, and the colloidal system did not exceed the theoretical limit of −30 mV boundary.[39] However, the Ag1 and Ag2 samples are qualitatively better because they retain the morphology of the individual NPs at a very similar ζ-potential to Ag3. The hydrodynamic diameters varied from 68 to 665 nm, but the largest values were linked with L3 leachates and macro-objects.

Dynamic light scattering (DLS) and TEM analyses confirmed the influence of organic compounds. The size distribution determined by DLS in Ag1 and Ag2 was in the 68−120 nm range; however, the TEM image analysis provided

5−15 nm "core diameters". In Ag3 samples, the large objects/aggregates were measured, and sizes above 200 nm were found.

The differences in the biomasses influence the NP core diameter calculations. Leachates from L1 and L2 biomasses provided a suitable environment for nanometric particles, and high-density agglomerates or macro-objects of NPs were synthesized in the L3 leachate.

Stability, Size Distribution, and Morphology Study of the Linden-like Modeled Samples. We investigated two model organic acids. The protocatechuic acid concentration provided the sum of measured phenolic concentrations, and the citric acid concentration gave the sum of all nonphenolic concentrations. We were then able to determine if these combined model acids are sufficient for NP's synthesis in the presence of trace Cl^-. The overall pH of the final organic mixtures was adjusted to 5.4 to mimic the natural pH of pure linden leachates (Table S4, Supporting Information).

There were several differences in these samples, similar to those in the linden-based samples. TEM analysis confirmed that AgM1, AgM2, and AgM3 contained mostly spherical Ag-AgCl NPs (Figure 2). The average NP size in the AgM1
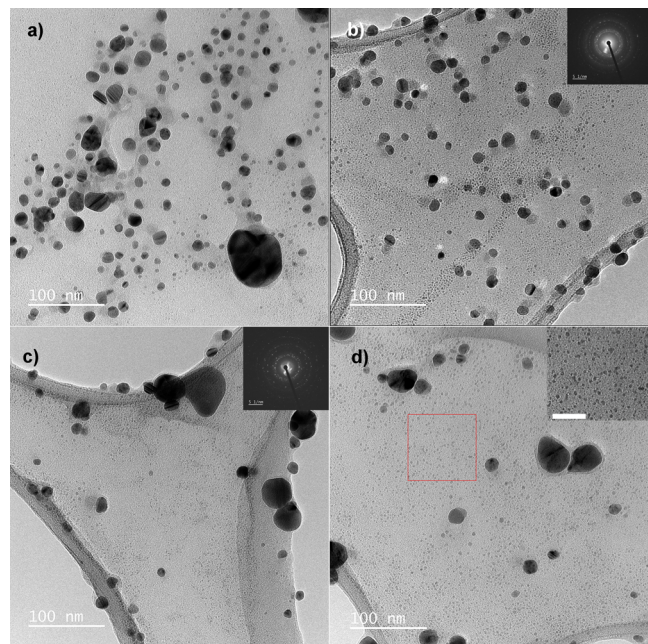

Figure 2. One sample was selected from each triplicate to illustrate the entire sample set. Spherical shapes of AgM1 were confirmed (a). Most "core" size diameters were from 10 to 15 nm; however, the fraction of 20−30 nm NPs was also present. The AgM2 sample (b) had similar nature to AgM1. TEM micrographs of AgM3 (c, d) revealed the big number of the small NPs about 4 nm (inset in d shows 4 nm NPs from the red square; scale bar, 30 nm). In all samples, larger objects were occasionally found and these were in the minority compared to small NPs.

sample was 13 ± 3 nm (Figure 2a), and the 14 ± 3 nm mean core size was found in the AgM2 sample (Figure 2b). Most values were in the 10−15 nm range, and large particles over 20 nm were also detected (Table 4).

The occurrence of approximately 5 nm NPs in the AgM2 sample was more obvious than in AgM1, and the AgM3 sample had bimodal size distribution, where most NPs fluctuated around 4 ± 1 nm with the occasional presence of 10−20 nm NPs (Figure 2c,d). Finally, larger objects were sometimes

obvious in all samples, but these were in the minority (Figure S1, Supporting Information).

All prepared samples had a negative ζ-potential value, while samples in the AgM1 set were the most stable; all were stable after 24 h (Table 4). The hydrodynamic diameters fluctuated between 3 and 112 nm, with the largest diameters observed in AgM1, and two size fractions were noted. The highest density of NP sizes around 14 nm was apparent in AgM2, while AgM3 had approximately 4 nm.

In addition, DLS measurements revealed that AgM3 had the lowest size and AgM1 had the highest size, and this correlates with TEM analyses. It is important here that the DLS values were evaluated as number counts, and the far less prevalent large NPs were excluded from the distribution.

We considered that Cl^- ions probably seeded subsequent NP nucleation because these ions are often added to reaction systems to initially provide very small uniform NPs. Here,[40] all twinned seeds in the polyol synthesis were removed from the solution by adding a small amount of Cl^- ions. This provided single-crystal seeds where nanocrystals prevailed.

Linden-Based Ag-AgCl Nanoparticle Phase Analysis. X-ray diffraction (XRD) analysis confirmed the presence of crystalline biphasic Ag-AgCl NPs in all colloidal samples (Figure 3a). Pure silver (PDF 00-004-0783) and chlorargyrite AgCl (PDF 01-085-1355) were identified, and both are cubic with an fcc lattice and $Fm3m$ space grouping. Differences among samples were observed in the presence of silver oxalate (PDF 00-022-1335), silver carbonate (PDF 00-031-1237), and the peak of the organic residues' presence. The silver oxalate phase close to 30° was confirmed in Ag2 samples, and small peaks between 33° and 34° proved the presence of silver carbonate in Ag2 samples with less certainty. Finally, the phase at approximately 27° may be organic in origin. Control samples L1−L3 were measured, and peaks indicative of crystalline phases were not detected (Figure S3a, Supporting Information).

Silver oxalate also appears in Ag3 samples, but the silver carbonate phase was not confirmed. Sample Ag1 contains the smallest number of additional phases, and the silver oxalate phase is likely found only in sample Ag1_3 (Figure S2a, Supporting Information).

Silver oxalate is a crystal that can be prepared by combining aqueous solutions of silver salts, oxalic acid, or soluble oxalates.[41] The oxalic acid source comes primarily from the leachate organic portion, and its formation and biosynthesis in plants have the following potential pathways: (1) The first pathway is the oxidation of glycolate and glyoxylate by glycolate oxidase. Glycolate oxidase is fairly abundant in green tissues, and potential substrates can be formed as a byproduct of photorespiration in photosynthetically active tissues. (2) The second pathway is the oxidation of oxaloacetate, presumably catalyzed by an oxaloacetase. (3) The last pathway is from L-ascorbic acid breakdown.[42,43]

Calcium oxalate is highly insoluble crystalline salt, which is formed in high plants from endogenous oxalic acid and calcium. Our study also confirms the high abundance of calcium oxalates (Figure 4a). The textured surface also includes the presence of trichomes and pollen grains (Figure 4b). The calcium oxalates herein were found as separate crystals (Figure 4c), and Figure 4d confirms that sufficient calcium provided the source for calcium oxalate growth. This is supported by our previous study, which established the high abundance of calcium oxalates,[44] and this druse crystal was a
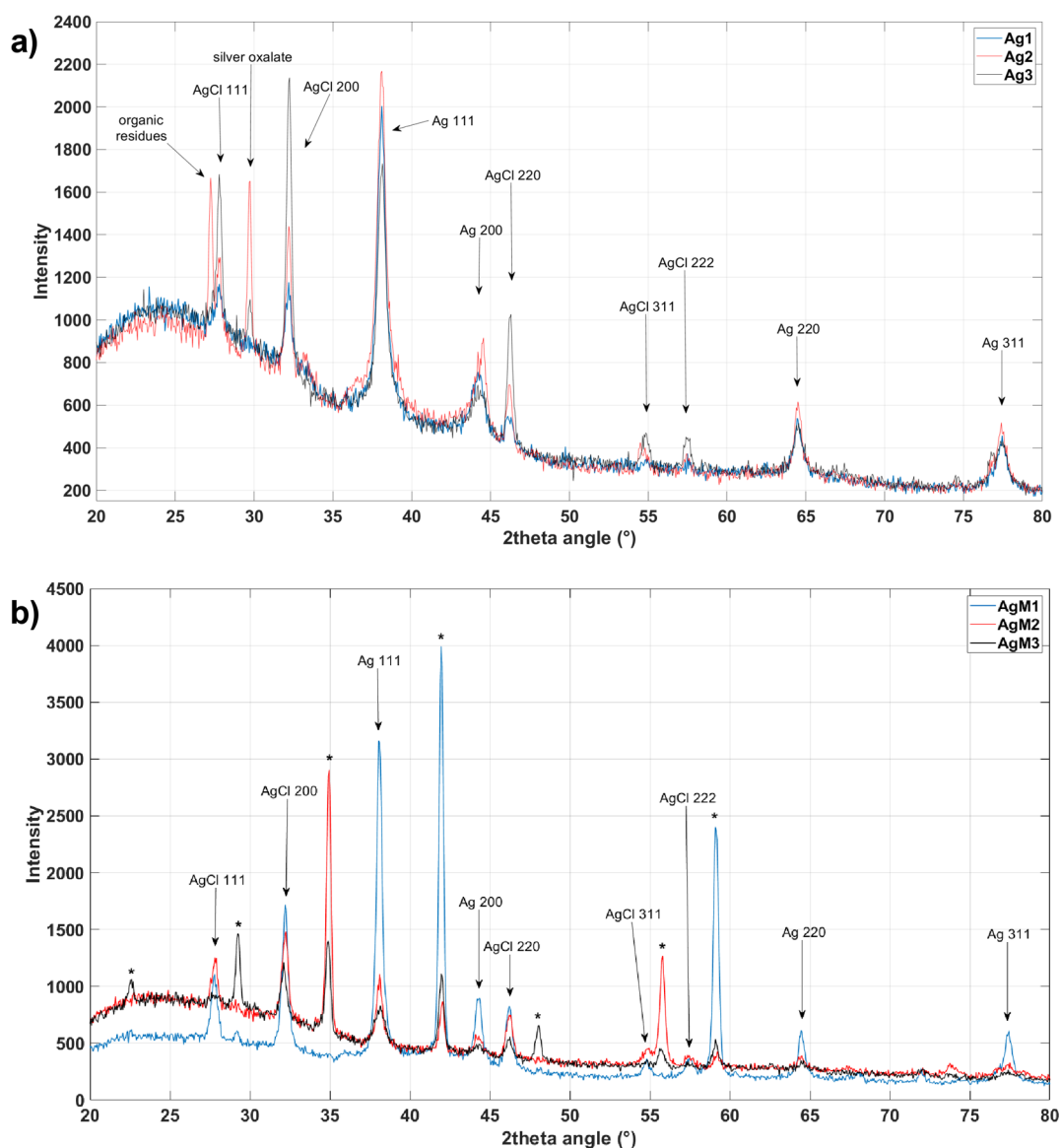
Figure 3. XRD patterns of all silver-based colloidal samples (a) were studied. The pure silver and chlorargyrite crystalline phases were confirmed, and additional phases most likely for silver oxalate, silver carbonate, and organic residues were also shown. Linden-like samples AgM1–AgM3 (b) contained pure silver and chlorargyrite crystalline phases with intensive peaks of silver nitrate (*).

typically multifaceted roughly spherical conglomerate and was present as a single crystal.[42]

The strongest diffraction maxima of silver oxalate were found in Ag2 samples, and this correlates with LC−MS data. Oxaloacetic acid is a possible precursor for oxalic acid biosynthesis, and its greatest concentration here was in the L2 biomass.

XRD analysis confirmed the highest chloride concentration in the Ag3 pattern. This indicates the significant peak at approximately 32° AgCl (200), and the results correlate with ion chromatography results discussed previously. Devi et al. confirmed the presence of Cl⁻ in the juice of *Aquilaria agallocha* leaves and subsequent formation of AgCl in the Ag-AgCl NP colloids.[45] Therefore, silver oxalate formation together with trace Cl⁻ ions can result in higher Ag⁺ ion consumption, and this indicates that Ag⁺ ions are used by these and most likely by other components during biosynthesis. As with many other green chemistry-mediated Ag NPs, the previously verified *Tilia* sp.-induced Ag-AgCl NPs confirmed

their antibacterial properties against pathogenic bacteria[46] and effectiveness in heterogeneous catalysis in *p*-nitrophenol decomposition.[44]

Linden-like Modeled Ag-AgCl Nanoparticle Phase Analysis. XRD analysis confirmed the presence of crystalline Ag-AgCl NPs in all colloidal samples (Figure S4, Supporting Information), and XRD patterns for AgM1, AgM2, and AgM3 were recorded in the 20−80° range (Figure 3b). The pure silver (PDF 01-089-3722) and chlorargyrite AgCl (PDF 01-085-1355) crystalline phases were identified with cubic, fcc lattice, and *Fm3m* space grouping. We also identified rhombohedral AgNO₃ peaks (PDF 01-070-0198). Here, the reaction most likely did not proceed to completion and AgNO₃ was not consumed. Finally, Figure S3b in the Supporting Information depicts the NaCl (PDF 00-005-0628) formed during trace Cl⁻ and Na⁺ precipitation. Figure 3b then highlights preferential precipitation to AgCl when the silver precursor is present.
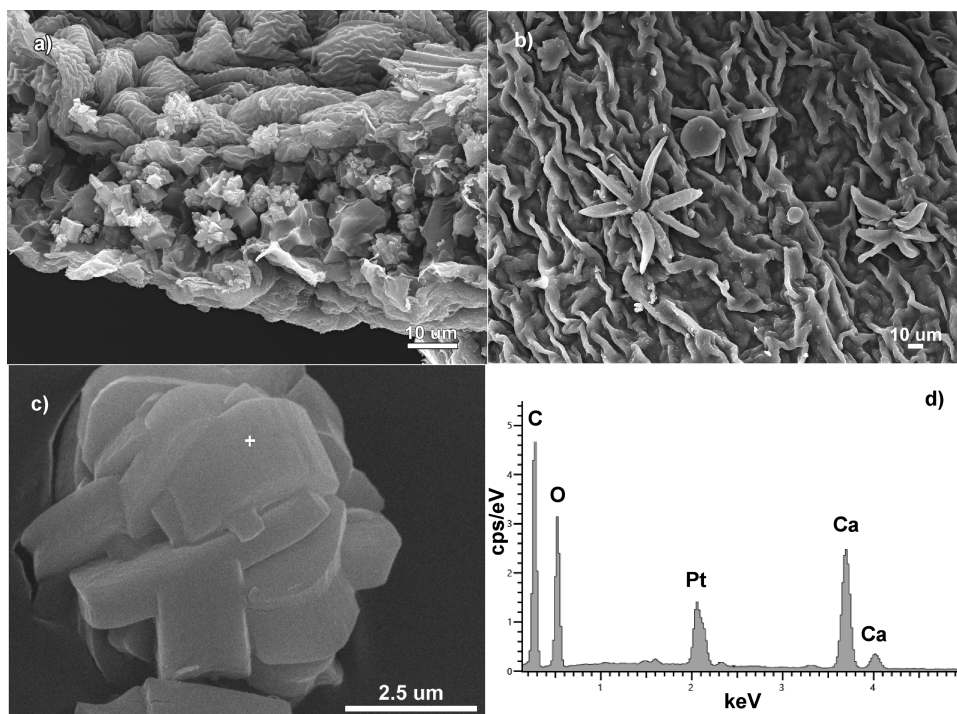
Figure 4. Dry linden biomass contains various organic and inorganic forms, including calcium oxalate crystals. A micrograph of linden blossom from the inflorescence shows a high abundance of calcium oxalates (a). The textured surface also includes the presence of trichomes and pollen grains (b). Calcium oxalates can also be found as separate crystals (c), and the EDS spectrum (d) confirms an amount of calcium, which is the source for calcium oxalate growth. The EDS spectrum was measured from the white-cross location on panel (c).

CONCLUSIONS

Leachates from *Tilia* sp. inflorescences were selected as the organic compound source for Ag-AgCl NP synthesis. Different Ag-AgCl NPs were successfully synthesized, and we found that their properties, such as size and stability, were highly influenced by biomass location, the concentration of phenolics, and the amount of organic acids. The second experiment selected the pure citric and protocatechuic acids as natural compounds identified in the linden leachates, and their concentrations were set as the value of phenolic/nonphenolic substances detected by LC−MS. We determined that NP sizes prepared from the linden differed from those artificially prepared.

The richer mixture of chemical compounds in the linden biomass most likely affected the overall reaction synthesis rate and resultant particle size. The system used in model reactions was simplified as much as possible to reduce the high number of different interactions between organic phases and silver ions. This is confirmed by XRD records, where we detected a silver oxalate crystal structure during linden-based synthesis. In contrast, the smallest particles in the modeled reactions are most likely caused by rapid precipitation.

The major advantage of our linden-based synthesis is the biomass availability for the preparation of large-volume NPs. This enabled easy handling and reproducibility when the process method and biomass remained uniform. In contrast, trace elements and the large amount of organic matter affected the reaction, and a change of substance content occurred with altered biomass location. This produced the expected differences in NP synthesis results. Although linden-like modeled mixtures proceed rapidly with a predominance of small and highly stable NPs, precise adherence to compound amounts is also required to achieve method reproducibility. These

Table 5. Labeling for Linden-Based Samples

sample description	abbreviation
pure leachate from LB1 (triplicate)	L1 (L1_1, L1_2, and L1_3)
pure leachate from LB2 (triplicate)	L2 (L2_1, L2_2, and L2_3)
pure leachate from LB3 (triplicate)	L3 (L3_1, L3_2, and L3_3)
Ag-AgCl nanoparticles prepared using pure leachate from L1 (triplicate)	Ag1 (Ag1_1, Ag1_2, and Ag1_3)
Ag-AgCl nanoparticles prepared using pure leachate from L2 (triplicate)	Ag2 (Ag2_1, Ag2_2, and Ag2_3)
Ag-AgCl nanoparticles prepared using pure leachate from L3 (triplicate)	Ag3 (Ag3_1, Ag3_2, and Ag3_3)

syntheses must also be further optimized because of the $AgNO_3$ presence in the samples.

All components contributing make it difficult to determine the precise biosynthesis mechanisms; however, we found that at least two organic components are sufficient for NP generation.

Finally, these research perspectives could be particularly beneficial in metal−polyol interactions, and they enhance the application of green chemistry-based metallic NPs by incorporating polymer nanofibers in the preparation of active antimicrobial matrices.

METHODS AND MATERIALS

Preparation of Silver Nanoparticles Using Different Linden Leachates. Ag-AgCl NPs were synthesized with inflorescences from the *Tilia* sp. deciduous tree collected from three different locations in the Moravian-Silesian region of the Czech Republic: Nová Ves u Frýdlantu nad Ostravicí (LB1), Klimkovice (LB2), and Hrabyně (LB3). This *Tilia* sp. is readily available in the geographical conditions of central Europe.

Table 6. Labeling for Linden-like Samples

sample description	abbreviation
control linden-like mixture 1 (triplicate)	M1 (M1_1, M1_2, and M1_3); CA:PrA ratio, 233:20 μg·mL^{-1}; Cl$^-$, 17 mg·L^{-1}
control linden-like mixture 2 (triplicate)	M2 (M2_1, M2_2, and M2_3); CA:PrA ratio, 268:9 μg·mL^{-1}; Cl$^-$, 17 mg·L^{-1}
control linden-like mixture 3 (triplicate)	M3 (M3_1, M3_2, and M3_3); CA:PrA ratio, 215:7 μg·mL^{-1}; Cl$^-$, 35 mg·L^{-1}
Ag-AgCl nanoparticles synthesized using linden-like mixture 1 (triplicate)	AgM1 (AgM1_1, AgM1_2, and AgM1_3)
Ag-AgCl nanoparticles synthesized using linden-like mixture 2 (triplicate)	AgM2 (AgM2_1, AgM2_2, and AgM2_3)
Ag-AgCl nanoparticles synthesized using linden-like mixture 3 (triplicate)	AgM3 (AgM3_1, AgM3_2, and AgM3_3)

The linden inflorescences were dried at 25 °C laboratory temperature for 5 days. For the preparation of linden leachate, 1.0 ± 0.1 g of dried plant and 50 mL of hot 80 °C deionized water were used. The plant was immersed in hot water for 5 min, and then the leachate was filtered through a 0.22 μm syringe filter (Whatman, USA). The purified leachate was then mixed with 10 mmol·dm^{-3} AgNO$_3$ initial precursor (≥99%, Ph. Eur., Carl Roth, Germany) in a 1:1 ratio. The final mixture was kept at 4 °C in the dark.[44] Samples were labeled according to the harvested biomass listed in Table 5, and all samples were prepared in triplicates.

Preparation of Silver Nanoparticles Using Modeled Linden-like Mixtures. We investigated two model organic acids. The protocatechuic acid concentration provided the sum of measured phenolic concentrations, and the citric acid concentration gave the sum of all nonphenolic concentrations.

Three different linden-like mixtures imitating natural linden leachates were prepared in DEMI water. We then used citric acid (CA; anhydrous ≥99.5%, p.a.) and 3,4-dihydroxybenzoic acid (protocatechuic acid, PrA; ≥ 97%; both from Carl Roth, Germany). HCl was chosen as the Cl$^-$ source (35%, Penta Chemicals, Czech Republic). This was diluted to specific concentrations chosen from ion chromatography data to mimic different Cl$^-$ levels in the natural leachates. The 1 M NaOH (Penta Chemicals, Czech Republic) solution provided pH adjustment to 5.4 for all samples. These mixtures were then used for NP synthesis in the same manner as the linden-based samples. Finally, all samples were prepared in triplicate, and the pure linden-like mixtures formed the control. The labeled samples are described in Table 6.

Morphology and Size Distribution. Ag-AgCl NPs prepared from L1−L3 leachates and modeled mixtures were characterized by a JEOL 2000 FX and HRTEM JEOL 2200FS (JEOL, Japan) with an SAED device; 2−3 μL of samples was placed on carbon lacey copper grids and dried. NP size distributions were evaluated by the JMicroVision program, and approximately 200 NPs from TEM micrographs were analyzed per sample. The final histograms were constructed using MATLAB software (MathWorks, USA).

The scanning transmission electron microscope JSM-7610F+ (JEOL, Japan) with EDS analysis was used for the observation of dry biomass observation. Before STEM analysis, the samples were placed on the carbon tape and sputtered with the thin Pt film.

The size distribution was measured in liquids by dynamic light scattering (DLS) followed by an evaluation of stability in a ZetaSizer Nano-ZS (ZEN 3600; Malvern Instruments Ltd., U.K.). All samples were measured in triplicate. pH measurements were maintained using an MPT-2 Multipurpose titrator (Malvern Instruments Ltd., U.K.) with 1% measurement error.

X-ray Diffraction. All liquid samples were adjusted prior to XRD measurement. Here, 600 μL of samples was slowly dried at 36 °C for 24 h to obtain a representative sample on a glass plate for XRD measurement. The XRD analysis was performed by a Bruker D8 DISCOVER diffractometer (Bruker AXS, Billerica, USA) equipped with a 12 kW X-ray tube with a rotating Cu anode at λ = 1.5418 Å. All measurements were in parallel beam geometry with a parabolic Goebel mirror in the primary beam. Finally, the X-ray diffraction patterns were recorded in grazing incidence in the 20−80° 2θ angular range, with 0.05° step size and α = 1.5° angle of incidence.

Chromatography Methods. *Ion Chromatography.* The selected inorganic components were identified by ion chromatography. The freshly prepared pure leachates were diluted 10 times with DEMI water, filtered through 0.45 μm membrane filters, and directly measured by Dionex ICS-5000 ion chromatography (Thermo Fisher, USA). This equipment comprises a pump that is able to create a gradient, a generator of Capillary EGC-KOH eluent, an AS autosampler, a 0.4 × 250 mm chromatographic column-IonPac AS19, a conductivity DC detector with an Anion Capillary Electrolytic Suppressor, and a Chromeleon chromatographic evaluation device. The optimized calibration curve then enabled chromatography evaluation, and standard deviations were provided by the evaluation software.

Liquid Chromatography with Mass Spectroscopy. The selected organic components were identified by LC−MS. The freshly prepared pure leachates were pipetted into filter vials and sequentially loaded into the chromatograph for analysis. The analysis was performed by an LC Agilent Technologies 1200 Series (Agilent, USA) connected to a triple quadrupole mass detector with ESI ionization. The system comprised an Agilent Technologies 1200 Series degasser, binary pump, autosampler, thermostat, diode array detector, and 6460 Triple Quad LC/MS quadrupole. Separation was then obtained using a 100 × 4.6 mm ZORBAX SC Poroshell EC-18 column (Agilent, USA) with 2.7 μm particle size.

The qualitative evaluation required comparison of the samples and standard retention times and calculation of the peak area using MassHunter software (Agilent, USA). Values are given for the final volumes of leachates from the leaching process. The default chromatographic analysis error is 3−5%; 5% deviation was included and was calculated using MS Excel.

■ ASSOCIATED CONTENT

ⓢ Supporting Information

The Supporting Information is available free of charge at https://pubs.acs.org/doi/10.1021/acsomega.1c05308.

Additional experimental data (DLS, stability, XRD, and size distributions) of separate samples and control samples (PDF)

■ AUTHOR INFORMATION

Corresponding Author

　Zuzana Šimonová − *Nanotechnology Centre, CEET, ENET Centre, CEET, and Department of Machining, Assembly and Engineering Metrology, Faculty of Mechanical Engineering, VSB−Technical University of Ostrava, Ostrava 708 00, Czech Republic;* ⊙ orcid.org/0000-0002-8397-3224; Email: zuzana.simonova@vsb.cz

Authors

　Veronika Krbečková − *Laboratory of Growth Regulators, Faculty of Science, Palacký University & Institute of Experimental Botany ASCR, Olomouc 783 71, Czech Republic*

　Zuzana Vilamová − *Nanotechnology Centre, CEET, VSB−Technical University of Ostrava, Ostrava 708 00, Czech Republic*

　Edmund Dobročka − *Institute of Electrical Engineering, Slovak Academy of Sciences, Bratislava 841 04, Slovak Republic*

　Bořivoj Klejdus − *Department of Chemistry and Biochemistry, Faculty of AgriSciences, Mendel University in Brno, Brno 613 00, Czech Republic*

　Miroslav Cieslar − *Department of Physics of Materials, Faculty of Mathematics and Physics, Charles University, Prague 121 16, Czech Republic*

　Ladislav Svoboda − *Nanotechnology Centre, CEET, VSB−Technical University of Ostrava, Ostrava 708 00, Czech Republic; IT4Innovations, VSB−Technical University of Ostrava, Ostrava 708 00, Czech Republic;* ⊙ orcid.org/0000-0001-9675-0604

　Jiří Bednář − *Nanotechnology Centre, CEET, VSB−Technical University of Ostrava, Ostrava 708 00, Czech Republic; IT4Innovations, VSB−Technical University of Ostrava, Ostrava 708 00, Czech Republic*

　Richard Dvorský − *Nanotechnology Centre, CEET, VSB−Technical University of Ostrava, Ostrava 708 00, Czech Republic; IT4Innovations, VSB−Technical University of Ostrava, Ostrava 708 00, Czech Republic*

　Jana Seidlerová − *Nanotechnology Centre, CEET, VSB−Technical University of Ostrava, Ostrava 708 00, Czech Republic; Department of Physical Chemistry and Theory of Technological Processes, Faculty of Materials Science and Technology, VSB−Technical University of Ostrava, Ostrava 708 00, Czech Republic*

Complete contact information is available at:
https://pubs.acs.org/10.1021/acsomega.1c05308

Author Contributions

Z.Š. performed the overall conceptualization, sample preparation, data management, and manuscript writing and editing. E.D. arranged the XRD analysis, B.K. performed LC−MS measurements and M.C. focused on TEM and SAED. Z.V. and R.D. guided ζ-potential and DLS measurements, V.K., J.B., and L.S. focused on data management and manuscript writing, and finally, J.S. performed the ion chromatography analysis and supervised the entire experiment.

Notes

The authors declare no competing financial interest.

■ ACKNOWLEDGMENTS

■ DEDICATION

This study is dedicated, in memoriam, to Prof. Bořivoj Klejdus.

■ REFERENCES

(1) Vukusic, P.; Sambles, J. R. Photonic Structures in Biology. *Nature* **2003**, *424*, 852−855.

(2) Siddiqi, K. S.; Husen, A.; Rao, R. A. K. A Review on Biosynthesis of Silver Nanoparticles and Their Biocidal Properties. *J. Nanobiotechnol.* **2018**, *16*, 14.

(3) Dauthal, P.; Mukhopadhyay, M. Noble Metal Nanoparticles: Plant-Mediated Synthesis, Mechanistic Aspects of Synthesis, and Applications. *Ind. Eng. Chem. Res.* **2016**, *55*, 9557−9577.

(4) Mittal, A. K.; Chisti, Y.; Banerjee, U. C. Synthesis of Metallic Nanoparticles Using Plant Extracts. *Biotechnol. Adv.* **2013**, *31*, 346−356.

(5) Oniszczuk, A.; Podgórski, R. Influence of Different Extraction Methods on the Quantification of Selected Flavonoids and Phenolic Acids from Tilia Cordata Inflorescence. *Ind. Crops Prod.* **2015**, *76*, 509−514.

(6) Karioti, A.; Chiarabini, L.; Alachkar, A.; Fawaz Chehna, M.; Vincieri, F. F.; Bilia, A. R. HPLC−DAD and HPLC−ESI-MS Analyses of Tiliae Flos and Its Preparations. *J. Pharm. Biomed. Anal.* **2014**, *100*, 205−214.

(7) Aguirre-Hernández, E.; González-Trujano, M. E.; Martínez, A. L.; Moreno, J.; Kite, G.; Terrazas, T.; Soto-Hernández, M. HPLC/MS Analysis and Anxiolytic-like Effect of Quercetin and Kaempferol Flavonoids from Tilia Americana Var. Mexicana. *J. Ethnopharmacol.* **2010**, *127*, 91−97.

(8) Truiča, G.; Teodor, E. D.; Radu, G. L. Organic Acids Assesments in Medicinal Plants by Capillary Electrophoresis. *Rev. Roum. Chim.* **2013**, *58*, 809−814.

(9) Jain, S.; Mehata, M. S. Medicinal Plant Leaf Extract and Pure Flavonoid Mediated Green Synthesis of Silver Nanoparticles and Their Enhanced Antibacterial Property. *Sci. Rep.* **2017**, *7*, 15867.

(10) Alavi, M.; Karimi, N. Biosynthesis of Ag and Cu NPs by Secondary Metabolites of Usnic Acid and Thymol with Biological Macromolecules Aggregation and Antibacterial Activities against Multi Drug Resistant (MDR) Bacteria. *Int. J. Biol. Macromol.* **2019**, *128*, 893−901.

(11) Vijayaraghavan, K.; Mahadevan, A.; Sathishkumar, M.; Pavagadhi, S.; Balasubramanian, R. Biosynthesis of Au(0) from

Au(III) via Biosorption and Bioreduction Using Brown Marine Alga Turbinaria Conoides. *Chem. Eng. J.* **2011**, *167*, 5.

(12) Vijayaraghavan, K.; Kamala Nalini, S. P. Biotemplates in the Green Synthesis of Silver Nanoparticles. *Biotechnol. J.* **2010**, *5*, 1098−1110.

(13) Jadhav, K.; Deore, S.; Dhamecha, D.; Hr, R.; Jagwani, S.; Jalalpure, S.; Bohara, R. Phytosynthesis of Silver Nanoparticles: Characterization, Biocompatibility Studies, and Anticancer Activity. *ACS Biomater. Sci. Eng.* **2018**, *4*, 892−899.

(14) Kuppusamy, P.; Ichwan, S. J. A.; Parine, N. R.; Yusoff, M. M.; Maniam, G. P.; Govindan, N. Intracellular Biosynthesis of Au and Ag Nanoparticles Using Ethanolic Extract of Brassica Oleracea L. and Studies on Their Physicochemical and Biological Properties. *J. Environ. Sci.* **2015**, *29*, 151−157.

(15) Geethalakshmi, R.; Sarada, D. V. L. Characterization and Antimicrobial Activity of Gold and Silver Nanoparticles Synthesized Using Saponin Isolated from Trianthema Decandra L. *Ind. Crops Prod.* **2013**, *51*, 107−115.

(16) Edison, T. J. I.; Sethuraman, M. G. Biogenic Robust Synthesis of Silver Nanoparticles Using Punica Granatum Peel and Its Application as a Green Catalyst for the Reduction of an Anthropogenic Pollutant 4-Nitrophenol. *Spectrochim. Acta, Part A* **2013**, *104*, 262−264.

(17) Saha, P.; Mahiuddin, M.; Islam, A. B. M. N.; Ochiai, B. Biogenic Synthesis and Catalytic Efficacy of Silver Nanoparticles Based on Peel Extracts of Citrus Macroptera Fruit. *ACS Omega* **2021**, *6*, 18260−18268.

(18) Equiza, M. A.; Calvo-Polanco, M.; Cirelli, D.; Señorans, J.; Wartenbe, M.; Saunders, C.; Zwiazek, J. J. Long-Term Impact of Road Salt (NaCl) on Soil and Urban Trees in Edmonton, Canada. *Urban For. Urban Greening* **2017**, *21*, 16−28.

(19) Drzewiecka, K.; Piechalak, A.; Goliński, P.; Gąsecka, M.; Magdziak, Z.; Szostek, M.; Budzyńska, S.; Niedzielski, P.; Mleczek, M. Differences of Acer Platanoides L. and Tilia Cordata Mill. Response Patterns/Survival Strategies during Cultivation in Extremely Polluted Mining Sludge - A Pot Trial. *Chemosphere* **2019**, *229*, 589−601.

(20) Sienkiewicz-Paderewska, D.; Dmuchowski, W.; Baczewska, A. H.; Brągoszewska, P.; Gozdowski, D. The Effect of Salt Stress on Lime Aphid Abundance on Crimean Linden (Tilia 'Euchlora') Leaves. *Urban For. Urban Greening* **2017**, *21*, 74−79.

(21) Chen, W.; He, Z. L.; Yang, X. E.; Mishra, S.; Stoffella, P. J. Chlorine Nutrition of Higher Plants: Progress and Perspectives. *J. Plant Nutr.* **2010**, *33*, 943−952.

(22) Wedin, W. F.; Struckmeyer, B. E. Effects of Chloride and Sulfate Ions on the Growth, Leaf Burn, Composition and Anatomical Structure of Tobacco (Nicotiana Tabacum L.). *Plant Physiol.* **1958**, *33*, 133−139.

(23) Matula, J. The Effect of Chloride and Sulphate Application to Soil on Changes in Nutrient Content in Barley Shoot Biomass at an Early Phase of Growth. *Plant, Soil Environ.* **2004**, *50*, 295−302.

(24) Cittan, M.; Altuntaş, E.; Çelik, A. Evaluation of Antioxidant Capacities and Phenolic Profiles in Tilia Cordata Fruit Extracts: A Comparative Study to Determine the Efficiency of Traditional Hot Water Infusion Method. *Ind. Crops Prod.* **2018**, *122*, 553−558.

(25) Ghodake, G.; Shinde, S.; Kadam, A.; Saratale, R. G.; Saratale, G. D.; Syed, A.; Shair, O.; Alsaedi, M.; Kim, D.-Y. Gallic Acid-Functionalized Silver Nanoparticles as Colorimetric and Spectrophotometric Probe for Detection of Al3+ in Aqueous Medium. *J. Ind. Eng. Chem.* **2020**, *82*, 243−253.

(26) Guo, D.; Dou, D.; Ge, L.; Huang, Z.; Wang, L.; Gu, N. A Caffeic Acid Mediated Facile Synthesis of Silver Nanoparticles with Powerful Anti-Cancer Activity. *Colloids Surf., B* **2015**, *134*, 229−234.

(27) Umadevi, M.; Bindhu, M. R.; Sathe, V. A Novel Synthesis of Malic Acid Capped Silver Nanoparticles Using Solanum Lycopersicums Fruit Extract. *J. Mater. Sci. Technol.* **2013**, *29*, 317−322.

(28) Mittal, A. K.; Kumar, S.; Banerjee, U. C. Quercetin and Gallic Acid Mediated Synthesis of Bimetallic (Silver and Selenium) Nanoparticles and Their Antitumor and Antimicrobial Potential. *J. Colloid Interface Sci.* **2014**, *431*, 194−199.

(29) Kim, D.-Y.; Suk Sung, J.; Kim, M.; Ghodake, G. Rapid Production of Silver Nanoparticles at Large-Scale Using Gallic Acid and Their Antibacterial Assessment. *Mater. Lett.* **2015**, *155*, 62−64.

(30) Dilshad, E.; Bibi, M.; Sheikh, N. A.; Tamrin, K. F.; Mansoor, Q.; Maqbool, Q.; Nawaz, M. Synthesis of Functional Silver Nanoparticles and Microparticles with Modifiers and Evaluation of Their Antimicrobial, Anticancer, and Antioxidant Activity. *J. Funct. Biomater.* **2020**, *11*, 76.

(31) Zhang, Y.; Liu, S.; Wang, L.; Qin, X.; Tian, J.; Lu, W.; Chang, G.; Sun, X. One-Pot Green Synthesis of Ag Nanoparticles-Graphene Nanocomposites and Their Applications in SERS, H2O2, and Glucose Sensing. *RSC Adv.* **2012**, *2*, 538−545.

(32) Petro-Turza, M. Flavor of Tomato and Tomato Products. *Food Rev. Int.* **1986**, *2*, 309−351.

(33) López-Bucio, J.; Nieto-Jacobo, M. F.; Ramírez-Rodríguez, V.; Herrera-Estrella, L. Organic Acid Metabolism in Plants: From Adaptive Physiology to Transgenic Varieties for Cultivation in Extreme Soils. *Plant Sci.* **2000**, *160*, 1−13.

(34) Dias, M. I.; Sousa, M. J.; Alves, R. C.; Ferreira, I. C. F. R. Exploring Plant Tissue Culture to Improve the Production of Phenolic Compounds: A Review. *Ind. Crops Prod.* **2016**, *82*, 9−22.

(35) Khokhar, S.; Owusu Apenten, R. K. Iron Binding Characteristics of Phenolic Compounds: Some Tentative Structure−Activity Relations. *Food Chem.* **2003**, *81*, 133−140.

(36) Atoui, A. K.; Mansouri, A.; Boskou, G.; Kefalas, P. Tea and Herbal Infusions: Their Antioxidant Activity and Phenolic Profile. *Food Chem.* **2005**, *89*, 27−36.

(37) Babenko, L. M.; Smirnov, O. E.; Romanenko, K. O.; Trunova, O. K.; Kosakivska, I. V. Phenolic Compounds in Plants: Biogenesis and Functions. *Ukr. Biochem. J.* **2019**, *91*, 5−18.

(38) Vilamová, Z.; Konvičková, Z.; Mikeš, P.; Holišová, V.; Mančík, P.; Dobročka, E.; Kratošová, G.; Seidlerová, J. Ag-AgCl Nanoparticles Fixation on Electrospun PVA Fibres: Technological Concept and Progress. *Sci. Rep.* **2019**, *9*, 15520.

(39) Doane, T. L.; Chuang, C. H.; Hill, R. J.; Burda, C. Nanoparticle ζ -Potentials. *Acc. Chem. Res.* **2012**, *45*, 317−326.

(40) Xia, Y.; Xiong, Y.; Lim, B.; Skrabalak, S. E. Shape-Controlled Synthesis of Metal Nanocrystals: Simple Chemistry Meets Complex Physics? *Angew. Chem., Int. Ed.* **2009**, *48*, 60−103.

(41) Boldyrev, V. V. Thermal Decomposition of Silver Oxalate. *Thermochim. Acta* **2002**, *388*, 63−90.

(42) Franceschi, V. R.; Nakata, P. A. Calcium Oxalate in Plants: Formation and Function. *Annu. Rev. Plant Biol.* **2005**, *56*, 41−71.

(43) Kobayashi, K.; Hattori, T.; Honda, Y.; Kirimura, K. Oxalic Acid Production by Citric Acid-Producing Aspergillus Niger Overexpressing the Oxaloacetate Hydrolase Gene OahA. *J. Ind. Microbiol. Biotechnol.* **2014**, *41*, 749−756.

(44) Konvičková, Z.; Holišová, V.; Kolenčík, M.; Niide, T.; Kratošová, G.; Umetsu, M.; Seidlerová, J. Phytosynthesis of Colloidal Ag-AgCl Nanoparticles Mediated by Tilia Sp. Leachate, Evaluation of Their Behaviour in Liquid Phase and Catalytic Properties. *Colloid Polym. Sci.* **2018**, *677*.

(45) Devi, T. B.; Begum, S.; Ahmaruzzaman, M. Photo-Catalytic Activity of Plasmonic Ag@AgCl Nanoparticles (Synthesized via a Green Route) for the Effective Degradation of Victoria Blue B from Aqueous Phase. *J. Photochem. Photobiol., B* **2016**, *160*, 260−270.

(46) Konvičková, Z.; Barabaszová, K. Č.; Holišová, V.; Kratošová, G.; Seidlerová, J. Phytosynthesis of Ag, ZnO and ZrO₂ Nanoparticles Using Linden: Changes in Their Physical-Chemical Nature Over Time. *J. Nanosci. Nanotechnol.* **2019**, *19*, 7926−7933.